A Comparative Study on Graphene Oxide and Carbon Nanotube Reinforcement of PMMA-Siloxane-Silica Anticorrosive Coatings

*Samarah V. Harb†, Sandra H. Pulcinelli†, Celso V. Santilli†, Kevin M. Knowles‡, Peter Hammer†**

† Instituto de Química, UNESP-Univ Estadual Paulista, 14800-060, Araraquara/SP, Brazil
‡ University of Cambridge, Department of Materials Science and Metallurgy, 27 Charles Babbage Road, Cambridge CB3 0FS, England

KEYWORDS: carbon nanotubes, graphene oxide, organic-inorganic nanocomposite, thermal and mechanical reinforcement, anticorrosive coating

ABSTRACT: Carbon nanotubes (CNTs) and graphene oxide (GO) have been used to reinforce PMMA-siloxane-silica nanocomposites, considered to be promising candidates for environmentally compliant anticorrosive coatings. The organic-inorganic hybrids were prepared by benzoyl peroxide (BPO) induced polymerization of methyl methacrylate (MMA), covalently

bonded through 3-(trimethoxysilyl)propyl methacrylate (MPTS) to silica domains, formed by hydrolytic condensation of tetraethoxysilane (TEOS). Single-walled carbon nanotubes and graphene oxide nanosheets were dispersed by surfactant addition and in a water/ethanol solution, respectively. These were added to PMMA-siloxane-silica hybrids at a carbon (CNT or GO) to silicon (TEOS and MPTS) molar ratio of 0.05%, in two different matrices, both prepared at BPO/MMA molar ratios of 0.01 and 0.05. Atomic force microscopy (AFM) and scanning electron microscopy (FEG-SEM) showed a very smooth, homogeneous and defect free surfaces of about 3 - 7 μm thick coatings deposited onto A1020 carbon steel by dip-coating. Mechanical testing and thermogravimetric analysis confirmed that both additives, CNT and GO, improved the scratch resistance, adhesion, wear resistance and thermal stability of PMMA-siloxane-silica coatings. Results of electrochemical impedance spectroscopy (EIS) in 3.5% NaCl solution, discussed in terms of equivalent circuits, showed that the reinforced hybrid coatings act as a very efficient anticorrosive barrier, with an impedance modulus up to 1 GΩ cm^2, about 5 orders of magnitude higher than the bare carbon steel. In the case of GO addition, the high corrosion resistance was maintained for more than 6 months in saline medium. These results suggest that both carbon nanostructures can be used as structural reinforcement agents, improving the thermal and mechanical resistance of high performance anticorrosive PMMA-siloxane-silica coatings, and thus extending their application range to aggressive environments.

INTRODUCTION

Since their discovery by Iijima [1] and Novoselov et al. [2], carbon nanotubes (CNTs) and graphene have stimulated intense activities in both fundamental and applied research areas. As a consequence of their outstanding mechanical, thermal and electrical properties, these carbon nanostructures have potentially a large number of applications in electronic devices, energy

storage systems, electrochemical electrodes and in the reinforcement of composite materials. Carbon nanotubes and graphene profit from their hexagonal sp^2 arrangements of carbon atoms, forming extremely stable cylindrical and monolayer structures, respectively. The thermal, chemical and mechanical resistance of CNTs and graphene are highly promising in the context of improving the properties of materials and extending their functionality.

To guarantee a reinforcement effect, the main challenge regarding the incorporation of CNTs and graphene into a host matrix is the ability to achieve their homogeneous dispersion by disaggregation of micrometric agglomerates, formed as a consequence of attractive van der Waals interactions between the 1D tubes or 2D layers, respectively. Several authors have studied an effective approach to separate the dense bundles into individual CNTs. Those methods, which proved to be most effective, are the use of surfactants and the linking of different functional groups to the nanotube walls [3,4]. A widely used strategy for incorporating graphene is the use of graphene oxide (GO) nanosheets. GO can be easily acquired from natural graphite flakes by acid treatment and due to the presence of epoxy, hydroxyl, and carboxyl functional groups on its basal planes, it can be stably dispersed in polar solvent, such as water and ethanol. For this reason, GO has attracted considerable attention as polymer filler [5].

Recent studies have shown that the inclusion of relatively small amounts of carbon nanotubes and graphene in polymer matrices results in a significant improvement in their mechanical strength [6-8] and thermal stability [6-10]. Mallakpour and Zadehnazari reported on the thermal and mechanical reinforcement of poly(amide-imide) (PAI) using multi-walled carbon nanotubes (MWCNTs) functionalized first with carboxylic groups and secondly with dopamine (MWCNT-Dop) [7]. The results indicate that MWCNT-Dop produced an increase of 21% in the thermal stability, 52% in the tensile strength and 65% in the Young's modulus, as the MWCNT-Dop

content increased from 0 to 15 wt.%. Similar results were obtained by Wang et al., using graphene as filler to poly(methyl methacrylate) (PMMA) matrix [8]. Compared with pure PMMA, PMMA/graphene composites showed improved mechanical properties (Young's modulus, tensile stress and elongation at break) and higher thermal stability.

Recent research activities involving the use of carbon nanostructures as fillers have been extended to the modification of composite materials applied as protective coatings of metallic alloys [11-15]. These composite materials face the challenge of being able to resist simultaneously severe situations such as high temperatures, abrasive conditions and corrosive environments. Recent reports on epoxy coatings containing 0.5 wt.% of CNT, deposited on 2024-T3 aluminum alloy, showed an improvement in adhesion strength and wear resistance, however their corrosion resistance did not increase significantly compared to those obtained for pure epoxy (10 kΩ cm^2) [12]. Another study on corrosion protection properties of epoxy/graphene composite coatings deposited on cold-rolled steel, repots only a moderate increase of the corrosion resistance of one order of magnitude compared to that of bare substrate (1 kΩ cm^2) [13]. Ramezanzadeh and coworkers grafted graphene oxide (GO) with a polyisocyanate (PI) resin, and subsequently incorporated 0.1 wt.% of PI/GO nanosheets into a polyurethane (PU) matrix, deposited on steel substrate [15]. They found that the incorporation of PI/GO into the PU matrix resulted in a significant improvement of the corrosion protection with impedance modulus values of up to 1 GΩ cm^2 after 30 days immersion in 3.5 wt.% NaCl solution. Despite of all these efforts, to our best knowledge there are no reports on simultaneous substantial improvement of mechanical, thermal and anticorrosive properties of protective coatings based on nanocomposites modified by carbon nanostructures.

The tendency of metal alloys to suffer corrosion in chemically aggressive environments, involving the spontaneous conversion of the metal to its original ore, is one of the most serious problems of the industrial age. In addition to the generation of significant amounts of waste, corrosion-induced damage results in huge economical losses, mainly related to replacement costs, and can lead to lack of serious safety problems due to the failure of critical components. Recent progress in material science has enabled new alloys and protective coatings to be developed, leading to a substantial retardation of the corrosion induced disintegration process, and thus reducing substantially the replacement and failure prevention costs. The development of new alloys is one important approach for inhibiting corrosion, but this is usually associated with high costs and requires the complete replacement of already installed metallic components. Protective organic coatings such as paints or resins, or inorganic coatings based on ceramic materials, represent a cheaper, easier and more efficient route for a significant improvement of durability of metallic parts, as they can be easily applied and provide a superior corrosion protection efficiency, in comparison with most alloys. Thus, for example, the Forth Bridge in Scotland has a triple layer glass flake epoxy paint coating expected to last 25 years, and it is routine to protect nickel-based superalloy turbine blades used in aerospace engines with thermal barrier coatings based on yttria-stabilized zirconia [16,17]. Despite of the advantages of these coatings, organic films often suffer from poor thermal and mechanical stability and a lack of adhesion, while most inorganic coatings present some degree of porosity and stress, leading potentially to cracks and adhesion failure of micron-thick films [18]. To overcome the limitations of ‘traditional’ coatings, organic-inorganic hybrids have been developed. Such materials present an intimate mixture of ceramic and polymeric phase on the molecular scale [19].

The PMMA-siloxane-silica hybrid system (PSS) is a class of organic-inorganic hybrid nanocomposites formed of a poly(methyl methacrylate) (PMMA) organic phase, covalently bonded to a silica network through siloxane (C-Si-O) bonds provided by the 3-(trimethoxysilyl)propyl methacrylate (MPTS), which acts as a coupling agent between the organic PMMA phase and inorganic silica phase. Recent studies have shown that this hybrid structure consists of dense silica cross-link nodes bridged by short PMMA chains, providing a dense nanocomposite, suitable for corrosion protection applications [18,20]. These optically transparent, dense and defect-free materials, prepared by the sol-gel process, have proved to be very efficient as protective coatings for metallic surfaces, showing a high corrosion resistance (impedance modulus > 10 GΩ cm^2), coupled with a long-term stability of more than 6 months in contact with 3.5% NaCl solution [20]. However, given the high fraction of the polymeric phase (>70 wt.%), the principal concern regarding the industrial applicability of PSS hybrids as protective coatings is related to their relatively low thermal and mechanical stability. To explore how this limitation can be overcome, MWCNTs functionalized by carboxylic groups have been added in a PSS hybrid at carbon to silicon ratios of 0.1, 1.0 and 5.0%. The results showed that CNTs did not affect the thermal stability of hybrid matrix of ~170 ºC and only slightly decreased the corrosion resistance (10 MΩ cm^2 in 3.5% NaCl solution) for the C/Si molar ratio of 5.0% [21]. However, in this study the mechanical properties of the CNT-loaded hybrids were not examined.

In this work, we demonstrate the feasibility to conjugate CNTs and GO with PMMA-siloxane-silica hybrids, resulting in a nanocomposite that combines improved mechanical and thermal stability with excellent anticorrosion properties, thus extending the field of application of these materials as protective coatings. The reinforcement effect has been confirmed by a number of

experimental techniques probing the thermal, mechanical and anticorrosive properties of the material.

EXPERIMENTAL METHODS

Carbon nanotubes dispersion. Single-walled carbon nanotubes (SWCNTs) were purchased from Dropsens. The catalytic chemical vapor deposition (CCVD) and a subsequent purification process yielded SWCNTs with diameter of 2 nm and length of several microns. Using the method of Alves da Cunha et al., the SWCNTs were dispersed in sodium dodecyl sulfate surfactant (SDS, Sigma-Aldrich) and hexadecanoic acid (palmitic acid, Sigma-Aldrich) [4]. 0.3 mg of CNTs were added to 10 mL of SDS 1% water solution and after 30 min in an ultrasonic bath, 110 mg of palmitic acid was added. After further 20 min of sonication, the solution was centrifuged for 3 h at 4000 rpm. The supernatant consisted of CNTs dispersed in SDS and palmitic acid with the non-polar part of these reagents interacting physically with the CNTs, while the polar groups interact with water, promoting the disentanglement of the nanotubes [4]. After dispersion, CNTs were added to the PMMA-siloxane-silica hybrid solution at a carbon (CNT) to silicon (MPTS and TEOS) molar ratio of 0.05%, in two different matrices (BPO0.01 and BPO0.05). These two CNT-loaded matrices were designated BPO0.01_CNT and BPO0.05_CNT, respectively.

Graphene oxide dispersion. Graphene oxide, provided by the Nanomaterials Laboratory (UFMG), was dispersed in a water/ethanol solution at 0.2 mg mL^{-1} concentration. The good dispersion of GO in water allowed the sol-gel preparation of a highly homogeneous hybrid nanocomposite. The dispersed GO was added to the hybrid inorganic phase, at a carbon (GO) to silicon (MPTS and TEOS) molar ratio of 0.05%, in two different matrices (BPO0.01 and

BPO0.05). These two GO-loaded matrices were designated BPO0.01_GO and BPO0.05_GO, respectively.

Nanocomposite synthesis. The synthesis was performed in three steps (Scheme 1): the first step consisted in the radical polymerization of methyl methacrylate (MMA, Sigma-Aldrich) with 3-(trimethoxysilyl)propyl methacrylate (MPTS, also known as TMSM, Sigma-Aldrich) using benzoyl peroxide (BPO, Sigma-Aldrich) as a thermal initiator and tetrahydrofuran (THF, Sigma-Aldrich) as the solvent. The reaction was maintained at 80 ºC for 4 h under reflux and constant stirring. In the second step, the sol-gel synthesis of the silica phase was performed, separately, by stirring a mixture of tetraethoxysilane (TEOS, Sigma-Aldrich), ethanol (Sigma-Aldrich) and water, acidified with nitric acid (pH 1), during 1 h at 25 ºC. Finally, the organic and inorganic components were mixed to produce a transparent and homogeneous PMMA-siloxane-silica solution.

The synthesis procedure and the molecular structures of TEOS, MPTS and MMA are shown in Scheme 1. The siloxane bridges (C-Si-O) between the organic and the inorganic phases are provided by MPTS, a modified silicon alkoxide with a methacrylate group, which acts as a coupling agent between the organic component, PMMA (polymerized MMA), and the inorganic silica phase. The molar ratios of following reagents were kept constant: MMA/MPTS = 8, TEOS/MPTS = 2, H_2O/Si = 3.5 and ethanol/H_2O = 0.5. The BPO/MMA molar ratio was kept at 0.01 and 0.05 to study the influence of the carbon nanostructures in two different matrices (BPO0.01 and BPO0.05).

Film deposition. First, A1020 carbon steel substrates (2.5 x 2.5 x 0.4 cm), having a nominal composition (wt.%) of C = 0.15%, Mn = 0.55 to 0.69%, Si = 0.13%, P = 0.03% and S = 0.01%, with the balance of Fe, were sanded using 100, 300, 600 and 1500 abrasive paper, washed with

isopropanol for 10 min in ultrasonic bath and dried under nitrogen. The hybrids solution was then used to coat the carbon steel substrates by dip-coating (3 immersions of 1 min, at a withdrawal rate of 14 cm min^{-1}, with intervals of 10 min air-drying). The remaining solution was placed in a Teflon holder to obtain unsupported films. Finally, all samples were cured at 60 °C for 24 h and subsequently at 160 °C for 3 h.

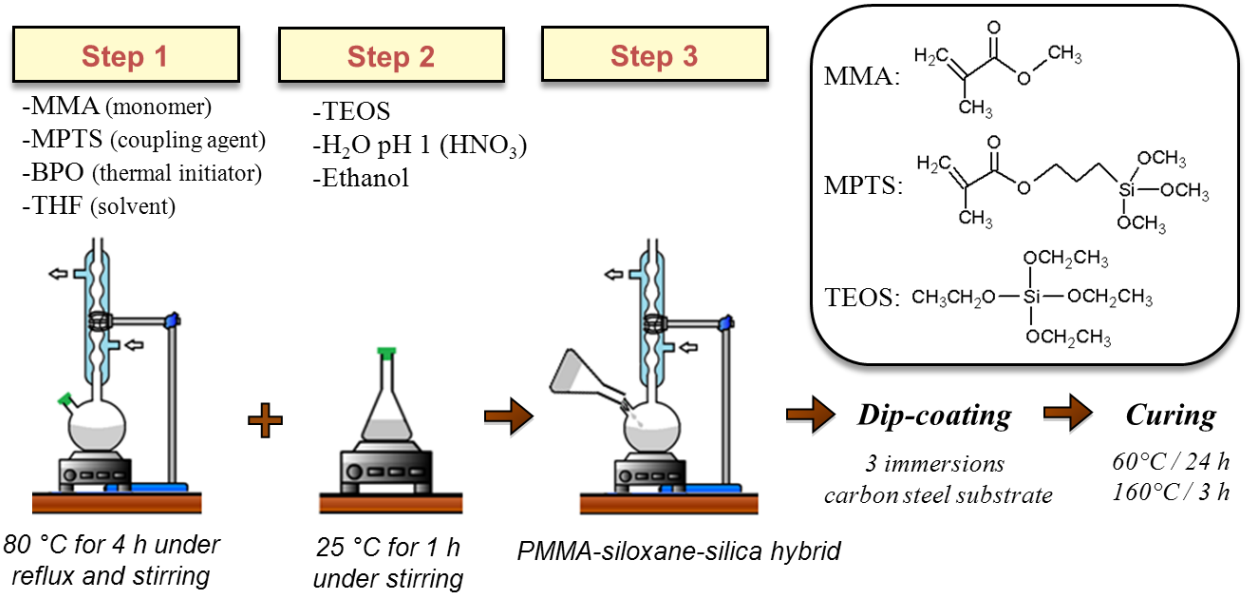

Scheme 1. Preparation conditions of the PMMA-siloxane-silica coatings and the molecular structures of precursors (inset).

Characterization. X-ray photoelectron spectroscopy (XPS) was used for characterization of the CNT and the GO carbon nanostructures. The measurements were performed in an UNI-SPECS UHV surface analysis system, using Mg Kα radiation (hν = 1253.6 eV) and a pass energy of 10 eV for high-resolution spectra. The CasaXPS software was used for the determination of the surface composition and for the deconvolution of the C 1s spectra, using a Shirley baseline and Voigt profiles. A field emission scanning electron microscope (FEG-SEM), JEOL 71500F, was used to obtain the morphology of the carbon nanostructures.

The coatings thickness was determined using Filmetrics F3-CS optical interference system. Atomic force microscopy (AFM) and FEG-SEM was performed to analyze the homogeneity and morphology of the surface of all hybrids coatings. For AFM, an Agilent Technologies 5500 atomic force microscope was used in tapping mode with a silicon cantilever. Root mean square (RMS) roughness values were obtained from a surface area of 1 μm^2, using the Gwyddion software. For electron microscopy (FEG-SEM), the coated steel samples were covered with a 16 nm evaporated gold layer to evaluate the morphology of the hybrid surface.

Thermogravimetric analyses (TGA) of unsupported films were carried out using a TA Instruments STD Q600 analyzer. For this, a quantity of 7 mg was heated at a rate of 5 ºC min^{-1} from 25 to 800 ºC, under 100 mL min^{-1} of nitrogen flow.

Microscratch measurements were performed at the National Physical Laboratory (NPL, Teddington, London, UK) using purpose-built equipment constructed at NPL. A spherical-conical diamond tip of 10 μm radius was applied to the coated substrates, with an increasing load from 2 mN to 100 mN on a 6 mm long track. For each sample, 3 scratches were performed to determine the average critical load for delamination, established using an optical microscope (Nikon Measuring Microscope MM-60).

Wear tests were carried out using the microscratch equipment by applying a constant load of 70 mN for 50 cycles on a 6 mm length track. The wear results were analyzed using an optical microscope (Nikon Measuring Microscope MM-60) and a confocal microscope (Olympus Confocal Scanning Laser Microscope LEXT OLS3100/OLS3000). Using the Gwyddion software, the 3D images of the wear track were used to extract for each sample 9 cross-section topographic profiles to obtain the average value of the tracks depth.

The anticorrosive efficiency of the hybrid coatings was investigated by electrochemical impedance spectroscopy (EIS) using a Gamry Potentiostat Reference 600. The impedance data were collected once a week until failure, over a frequency range from 10^{-2} Hz to 10^{4} Hz, using 80 mL of NaCl 3.5% standard solution at 25 °C, 10 points per decade and an amplitude of 10 mV (rms), after checking the open circuit potential (OCP) for 5 min. The coated carbon steel was used as working electrode, Ag|AgCl|KClsat served as reference electrode and a platinum mesh was used as counter electrode. A fourth platinum electrode connected to reference thought a 0.1 μF capacitor was used to avoid high-frequency phase shifts. To guarantee the reproducibility of the results, all electrochemical measurements were performed in duplicate. The EIS lifetime of the coating was defined as the time span until a significant drop of the corrosion resistance occurred.

The experimental data were fitted with an equivalent circuit to obtain a deeper insight into the electrochemical properties of the electrolyte/coating/substrate system. As the capacitive element does not behave ideally it was represented by constant phase elements (CPE). The effective capacitance of the coating can be calculated by:

$$C = Q^{1/n} R^{(1-n)/n} \qquad \text{Eq. 1}$$

where Q and n are CPE parameters, and R is the coating resistance [22].

CPE becomes equal to a capacitance for n = 1, equal to a resistance for n = 0, and equal to an inductance for n = −1 [23]. After extracted the coating capacitance, the volume fraction of water uptake, ϕ, of the coating was calculated using the Brasher-Kingsbury relation [24]:

$$\phi(\%) = \frac{\log\left(\frac{C_t}{C_0}\right)}{\log(\varepsilon_w)} \times 100 \qquad \text{Eq. 2}$$

where C_t is the coating capacitance at time t, C_0 is the initial coating capacitance and ε_w is the dielectric constant of water at the working temperature. As the measurements were performed at 25 °C the value of dielectric constant of water used was taken to be 78.3 [25].

RESULTS AND DISCUSSION

Morphology and bonding structure of CNTs and GO. Excluding the presence of hydrogen, the quantitative XPS analyses have shown that the raw CNTs are composed of 93.2 at.% of carbon and 6.8 at.% of oxygen, while the GO structure contains 70.6 at.% of carbon, 28.5 at.% of oxygen and traces of contaminants (0.4 at.% of nitrogen, 0.1 at.% of silicon and 0.3 at.% of sulfur). As expected the XPS C 1s spectra of the CNTs (Figure 1a) showed a predominant aromatic C–C sp^2 component, smaller contributions associated with sp^3 carbon (C–H), ether/alcohol (C–O), carbonyl (C=O) and carboxyl (O–C=O) groups, as well as the characteristic π plasmon transitions, related to collective oscillations of valence electrons of the hexagonal lattice. The C-C sp^2 component, related to aromatic bonds (284.4 eV), has a high intensity (65.0%) and narrow FWHM (0.9 eV), which scale with the high degree of order of the hexagonal carbon structure [26]. The C 1s spectrum of GO displays a strong contribution of C-O groups and a pronounced presence of C=O and O-C=O bonds, inserted by acidic treatment into the hexagonal carbon planes (Figure 1b).

Raw CNTs are found in the form of dense bundles due to van der Waals interactions between the individual carbon tubes. The applied procedure using SDS surfactant and palmitic acid promoted a disentanglement of the dense clusters leading to a homogeneous dispersion of individual carbon nanotubes (Figure 1c). As can be observed in Figure 1d, the GO nanoflakes dispersed in an ethanol/water solution have an average size of 25±5 nm.

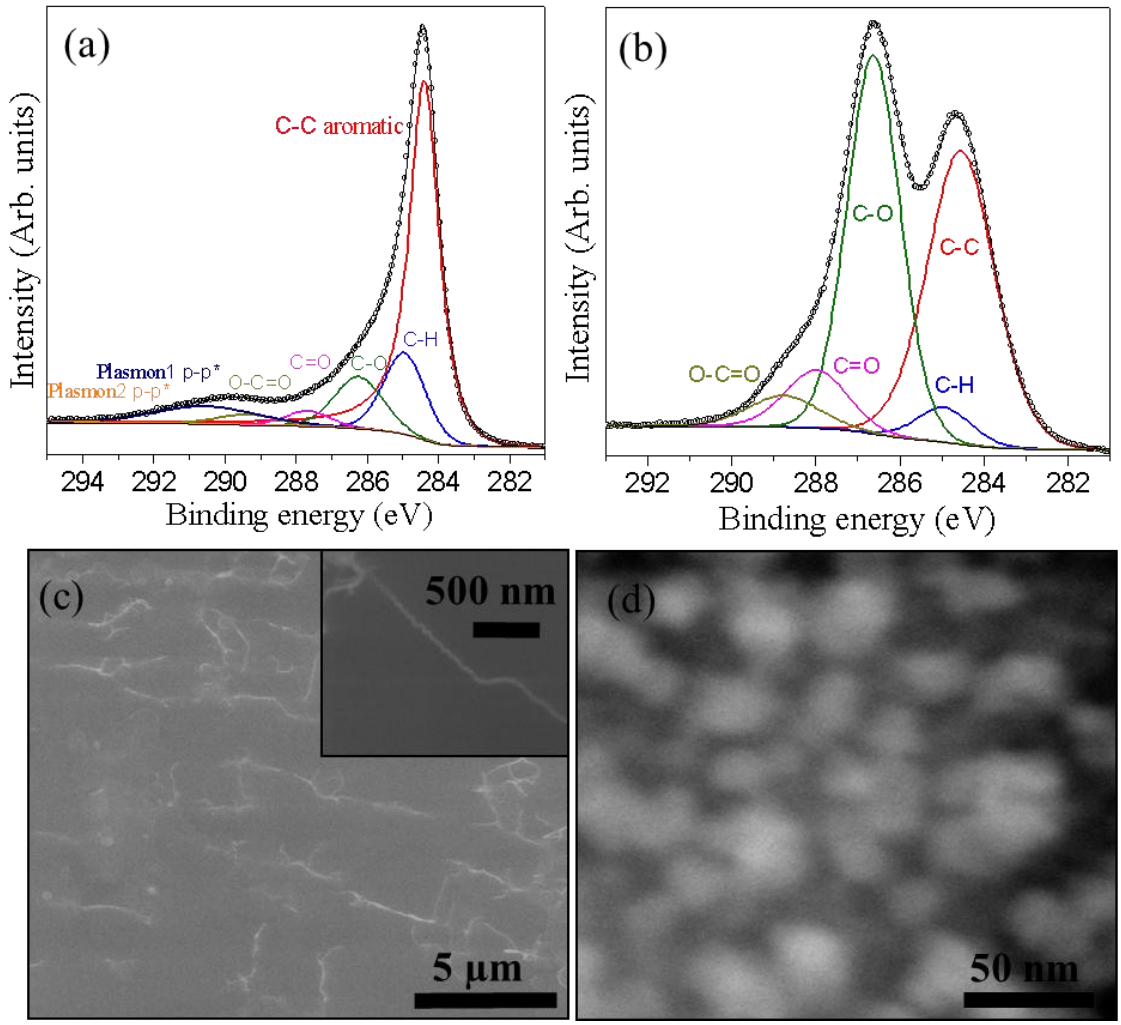

Figure 1. C 1s XPS spectra of as-received CNTs (a) and GO (b). FEG-SEM micrograph of CNTs dispersed with SDS surfactant and palmitic acid (c), and GO dispersed in an ethanol/water solution (d).

Hybrid morphology. Polymethyl methacrylate (PMMA) can be obtained by a variety of polymerization mechanisms, from which the most common is the polymerization of the methyl methacrylate monomer using a thermal initiator. Since the function of BPO as a thermal initiator is to produce radicals that initiate the polymerization process, the main effect caused by increasing BPO content was an enhanced polymerization rate. This leads to a reduction of

gelation time and a more viscous solution, and consequently to thicker coatings. Moreover, the addition of GO and CNTs also contributed to a higher viscosity of the solution, thus increasing the thickness of the coatings (Table 1). In addition, it is important to note that a higher degree of polymerization may have important implications on the thermal and mechanical stability of the formed nanocomposite.

Table 1. Properties of PMMA-siloxane-silica coatings modified with CNTs and GO: film thickness obtained by optical interferometry, surface roughness extracted by AFM images, critical load for delamination obtained by microscratch measurements, average depth of the wear tracks, open circuit potential (OCP) measured after one day immersed in 3.5% NaCl solution and coating lifetime in 3.5% NaCl solution.

sample	thickness (µm)	RMS roughness (nm)	critical load (mN)	track depth (µm)	OCP (mV)	EIS lifetime (days)
BPO0.01	2.8	0.4	78	3.0	196	56
BPO0.01_CNT	5.7	0.4	---	2.1	246	43
BPO0.01_GO	3.1	0.3	94	3.1	227	203
BPO0.05	3.5	0.4	84	---	248	21
BPO0.05_ CNT	6.6	0.5	133	---	582	7
BPO0.05_GO	5.5	0.5	148	---	198	168

All PMMA-siloxane-silica hybrid coatings on carbon steel were colorless, transparent and presented a very uniform and defect free surface. A representative image of the coated samples is shown in Figure 2a. Inspections by FEG-SEM and AFM, performed for all hybrid coatings, confirmed their homogeneity and the absence of micrometric agglomerates of CNTs and GO (Figure 2b and 2c). In addition, the AFM analysis confirmed the smoothness of the surface of the coatings (Figure 2c) with extremely low RMS roughness values (≤ 0.5 nm), listed in Table 1.

Recently we reported on the structural properties of PMMA-siloxane-silica nanocomposites and the results showed that the hybrid nanostructure consists of a dense network of ramified

silica-siloxane cross-link nodes, with an average radius of 0.8 nm, covalently interconnected by short PMMA chains over an average distance of 4.6 nm [20]. Hence, the smooth surface is indicative of the small size of the building blocks of the system, showing no significantly change after incorporation of CNTs and GO additives.

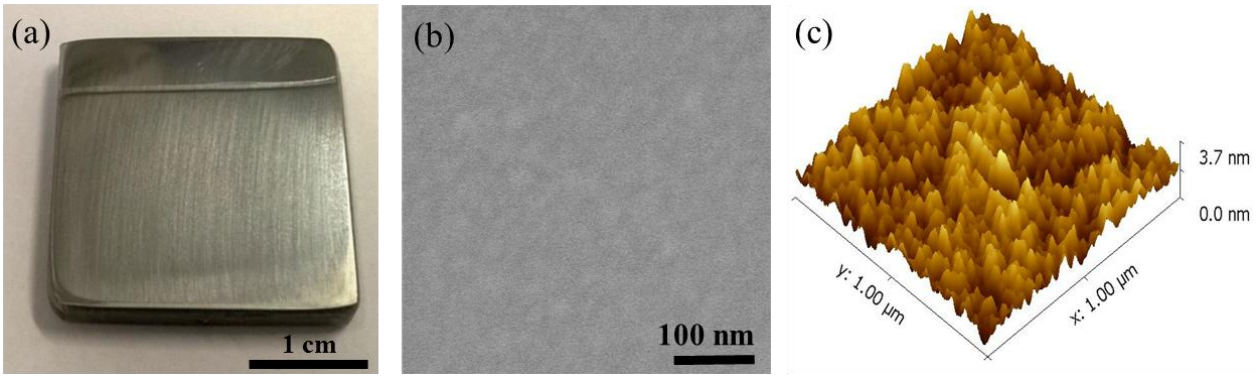

Figure 2. Representative image (a), FEG-SEM micrograph (b) and AFM map (c), obtained for the BPO0.01_CNT coating deposited on carbon steel.

Thermal analysis. Thermogravimetry curves (TG) and differential thermogravimetry curves (DTG) for all samples are shown in Figure 3. These curves provide information on the thermal stability and consequently on the overall connectivity of the hybrid nanocomposites. Three events of thermal degradation can be identified in the DTG plots (Figure 3b and 3c): the small narrow peak around 220 ºC (T_1) indicates the scission of inherently weak head-to-head linkages of the PMMA polymer, the shoulder of the main peak around 310 ºC (T_2) corresponds to vinylidene chain-end initiation, and the main event at about 400 ºC (T_3) arises from depolymerization of head-tail segments [27,28]. In addition, the weak signal at ~500 ºC (T_4) is related to the dehydration of remaining silanol groups of the silica network [27]. The temperatures at which the rate of mass loss is a maximum (T_1, T_2 and T_3) are listed in Table 2,

together with the 5% weight loss temperatures (T_0), marking the thermal stability of the hybrid, and the residue at 800 ºC.

The results show clearly that the addition of CNTs and GO into the BPO0.01 matrix, and, to a lesser extent, to the BPO0.05 matrix, improves the thermal stability of the hybrids. For BPO0.01 the onset of thermal degradation (T_0) increased by 15 ºC and 70 ºC in presence of CNTs and GO, respectively, and all depolymerization events were suppressed and shifted to higher temperatures. This result is more pronounced than the 30 °C shift of T_0, observed by Jin et al [29] for PMMA containing 26 wt.% of CNTs. The authors attributed the retardation effect to interactions between the carbon nanostructure and macroradicals generated during the depolymerization process. A shift of the non-oxidative onset of degradation in the range of 10 - 30 °C has been reported for GO-based fillers [30]. Pham et al. [31] found a thermal retardation effect of 10 ºC for 1.0 wt.% of reduced GO in PMMA matrix, which they attributed to a barrier effect of GO, inhibiting the emission of decomposition products. Consequently, the incorporation of GO-derived fillers can significantly reduce gas permeation through a polymer composite due to the formation of a 'tortuous path' along the GO platelets, hindering molecular diffusion through the matrix, and thus providing an improved thermal resistance of the material [30, 32].

Besides the radical scavenging and barrier effects, the remarkable increase of the thermal stability of PSS hybrids containing carbon nanostructures can be explained by the flame-retardant effect of the CNTs and GO nanostructures [33,34]. During decomposition, the flammable polymeric phase forms in the presence of the carbon nanostructures a carbonaceous char structure, which acts as diffusion barrier and thermal insulator [35]. The higher residue percentage observed for the BPO0.01_CNT and BPO01_GO samples hints on the role of GO and CNT in the char formation, which hinders the diffusion of volatile species and contributes to

the enhances of the thermal stability of the material. In comparison with CNTs, the two-dimensional GO geometry might be more favorable for the improvement of the thermal properties of the hybrid nanocomposite.

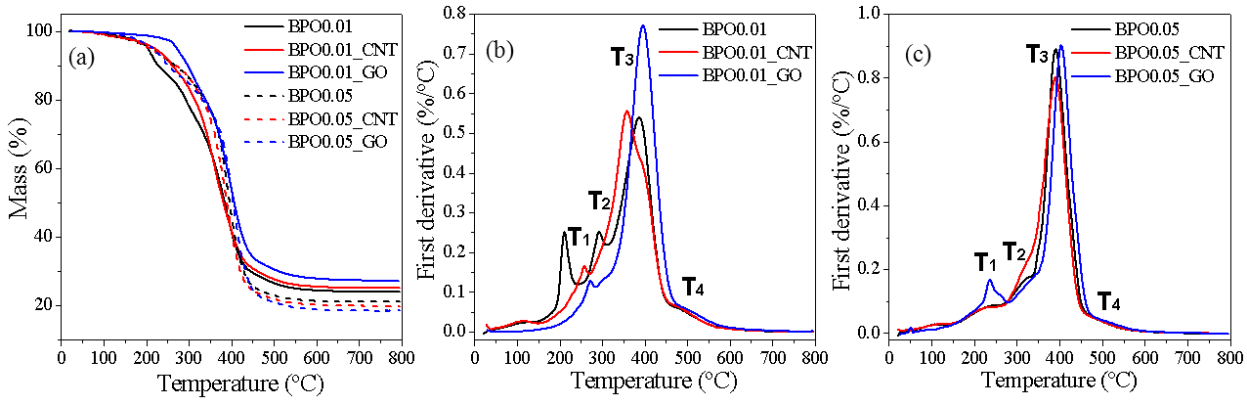

Figure 3. Thermogravimetry curves of all PMMA-siloxane-silica hybrids (a), and differential thermogravimetric curves of BPO0.01 hybrids (b) and BPO0.05 hybrids (c).

Table 2. The characteristic parameters of the hybrid thermal degradation in N_2 atmosphere: temperature of 5% weight loss (T_0), temperatures of the first (T_1), second (T_2) and third (T_3) degradation event (see text), and the percentage of the residue at 800 °C.

sample	T_0 (°C)	T_1 (°C)	T_2 (°C)	T_3 (°C)	residue (wt.%)
BPO0.01	205	210	290	385	24.0
BPO0.01_CNT	220	255	355	405	25.1
BPO0.01_GO	275	270	suppressed	395	27.1
BPO0.05	208	220	310	390	21.1
BPO0.05_ CNT	209	220	310	390	19.8
BPO0.05_GO	216	235	310	405	18.4

Mechanical properties. For industrial applications, protective coatings should be able to increase the lifetime of the metal substrate in abrasive and corrosive environments, ensuring that film detachment, scratch or wear failure does not occur, thus preventing that the electrolytes access the undelaying metal surface. The microscratch technique is a fast, effective and widely

used method to assess the mechanical performance of thin films and the coating/substrate adhesion strength. A scratch resistant material presents a high coefficient of friction, hindering the penetration of the scratch tip into the material, while a strongly adherent coating has a high critical load for delamination due to the strong bonding at the coating/substrate interface. In the case of PSS hybrids the adhesion between coating and carbon steel is the consequence of the covalent interaction between the hydroxyl groups of the substrate and the silanol groups of the inorganic part of the hybrid.

The scratch resistance and adherence of all coatings were tested by sliding a diamond tip under increasing load on a 6 mm track until film detachment (Figure 4), marked as critical load of delamination (Table 1). The critical values were accessed by optical examination of the scratch track, divided in 5 intervals: 0.0 mm (starting point), 1.5 mm, 3.0 mm, 4.5 mm and 6.0 mm (end point), marking a load of 100 mN (Figure 5).

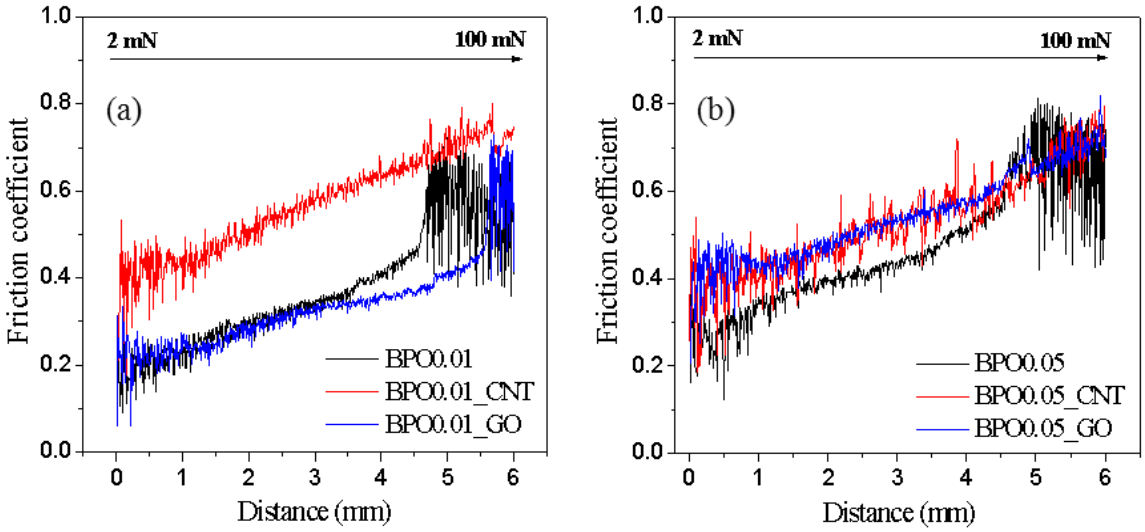

Figure 4. Microscratch curves obtained for unloaded and CNT and GO loaded PMMA-siloxane-silica coatings deposited on A1020 carbon steel for (a) BPO0.01 matrix and (b) BPO0.05 matrix.

The results obtained indicate that BPO0.01 and BPO0.05 were the softest and less adherent coatings, each showing four deformation stages with increasing force: (1) elastic deformation, (2) plastic deformation (3) cracks and (4) delamination, marked in Figure 5. For these two coatings, the coefficient of friction increased from 0.2 to 0.4 during the test and the critical loads of delamination were 78 mN and 84 mN for the BPO0.01 and BPO0.05 matrix, respectively. The BPO0.01_CNT coating showed the highest reinforcement effect. Here, no delamination was observed up to 240 mN, the maximum load of the equipment (Figure 6a). It is remarkable that for the BPO0.05_CNT and BPO0.05_GO coatings a load of 100 mN was not sufficient to induce delamination. The critical loads of BPO0.05_CNT and BPO0.05_GO coatings were 133 mN and 148 mN (Figure 6b and 6c), respectively, also having 0.1 to 0.2 units higher friction coefficient (Figure 4). The higher scratch resistance coupled with 2 – 3 fold increases in the critical loads for delamination are related to the contribution of intrinsic mechanical properties of CNT and GO, leading to a significant improvement of the coatings.

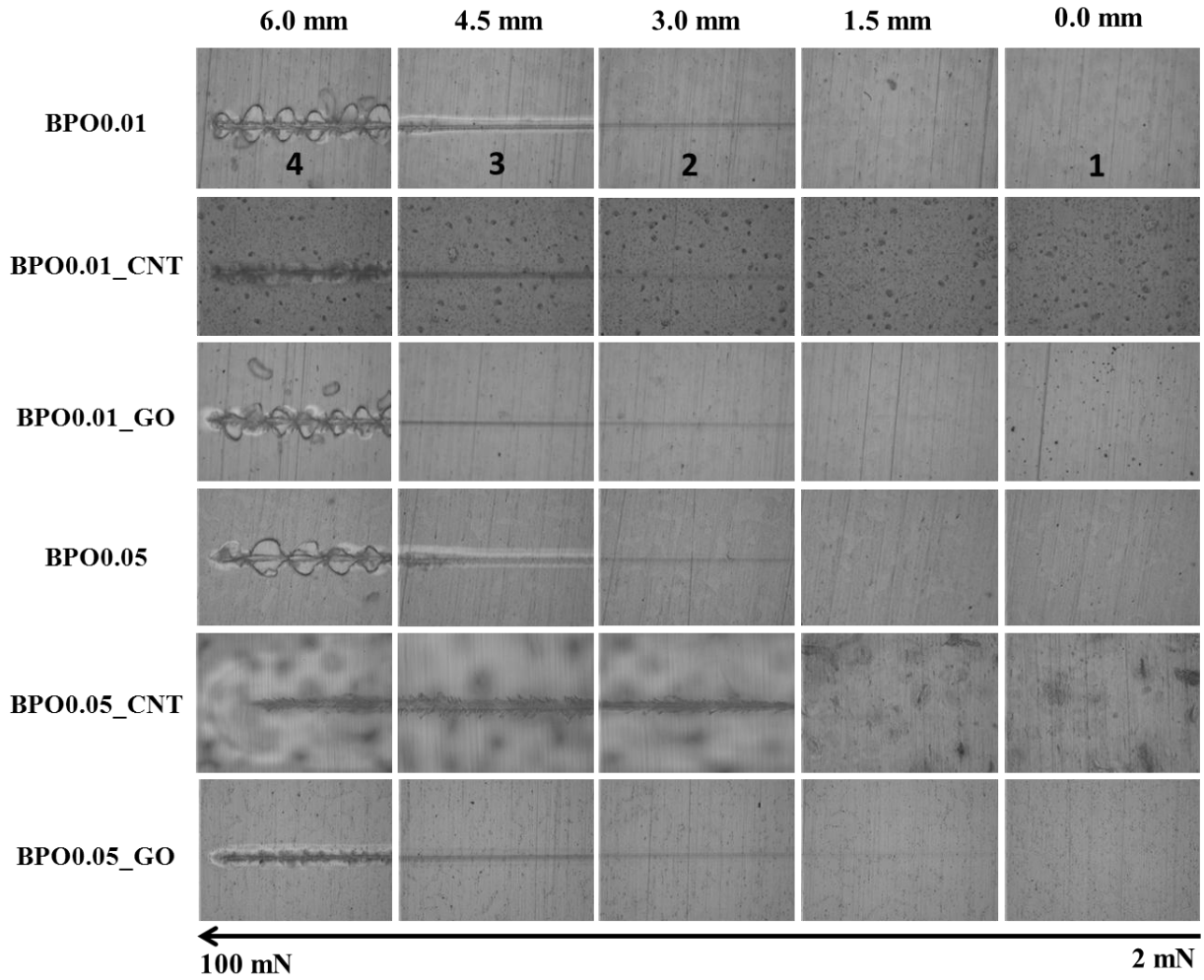

Figure 5. Optical micrographs after scratch test of unloaded and CNT and GO loaded PMMA-siloxane-silica coatings deposited on A1020 carbon steel.

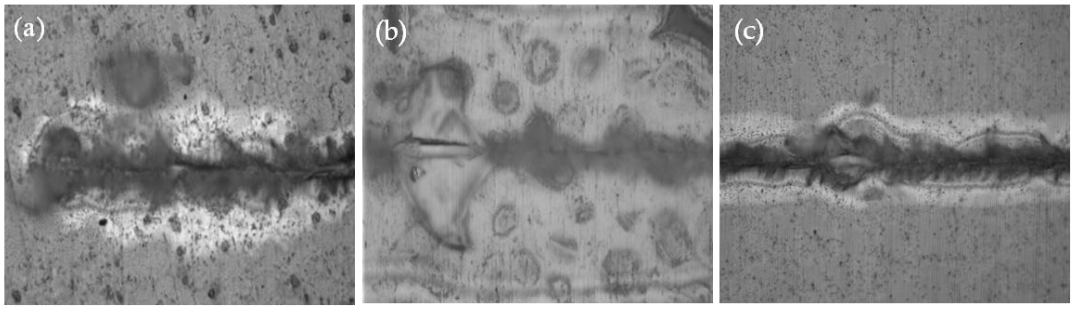

Figure 6. Optical micrographs of the BPO0.01_CNT coating after scratch testing up to a load of 240 mN (a), BPO0.05_CNT coating after scratch testing up to a load of 133 mN (b), and BPO0.05_GO coating after scratch testing up to a load 148 mN (c).

The wear resistance of the three BPO0.01 matrix coatings was determined by analysis of the wear tracks by optical and confocal optical microscopy, after applying 50 scratch cycles at a load of 70 mN (Figure 7). The positive values of the friction coefficient correspond to scratching to the right and the negative values correspond to scratching to the left. The BPO0.01 and BPO0.01_GO coatings showed a variation of their friction coefficient between 0.3 - 0.6, accompanied by the formation of cracks along the wear track, and a average track depth of 3.0±0.2 μm and 3.1±0.3 μm, respectively, while the BPO0.01_CNT sample displayed a constant coefficient of friction of 0.6 and ended the wear test after 50 cycles with a smooth and less deep track of 2.1±0.2 μm. The average scratch depth observed for BPO0.01 and BPO0.01_GO sample indicates that the metal substrate was reached, while the depth of the BPO0.01_CNT remained noticeably smaller than the coating thickness of 5.7 μm (Table 1), highlighting the beneficial effect of the CNT nanosized filler. The higher friction coefficient of the BPO0.01_CNT hybrid, remaining constant value over the 50 scratch circles, suggest that the homogeneously dispersed CNTs act as rigid obstacles for the wear tip, thus improving significantly the wear performance of the coating.

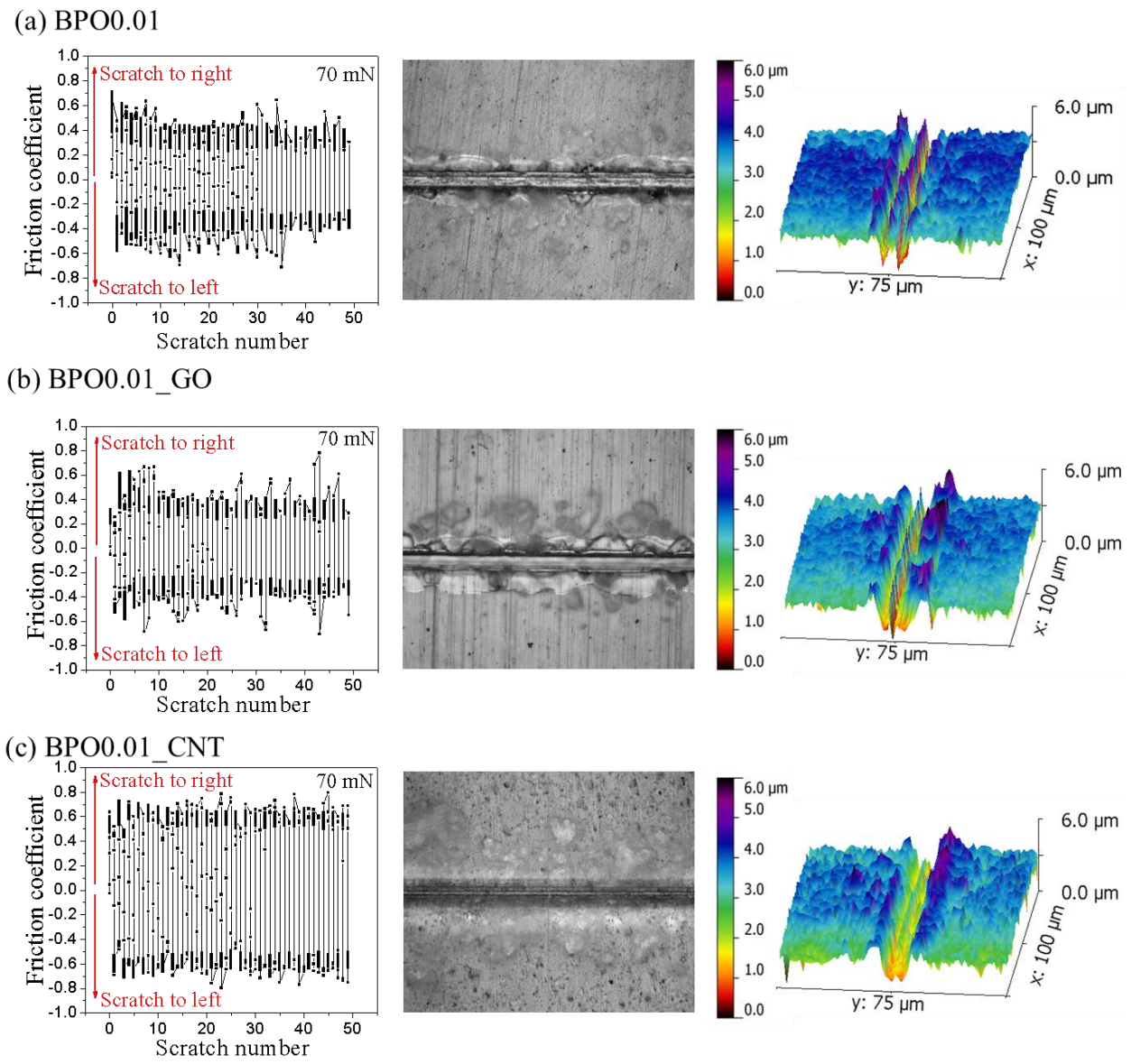

Figure 7. Friction coefficient as a function of the scratch number, optical micrograph of the wear track and confocal optical micrograph of the wear track of the BPO0.01 (a), BPO0.01_GO (b) and BPO0.01_CNT (c) of PMMA-siloxane-silica hybrid coatings.

Anticorrosive properties. The corrosion resistance of the coatings was determined using electrochemical impedance spectroscopy in an unaerated 3.5 % NaCl standard saline solution at room temperature. Before each EIS data acquisition, the open circuit potential (OCP) was

measured over a period of 5 min. The OCP values of all coated carbon steel samples, determined after one day of immersion in saline environment, are shown in Table 1. All coated samples had extremely stable OCP values, which were shifted significantly into the passive potential region in comparison with the -718 mV OCP of the carbon steel substrate.

All impedance measurements were performed once a week until the observation of a significant drop in the impedance modulus, associated with the appearance of localized corrosion in form of pitting. The corresponding time span values, referred as EIS lifetime of the coating, are listed in Table 1. Figure 8 shows the Nyquist and Bode plots for all hybrid coated samples after one day of immersion in saline environment. The Bode plot of the pure BPO0.01 matrix had an impedance modulus of 0.1 GΩ cm^2, remaining almost unchanged during 56 days of the coating lifetime, while the BPO0.05 coatings had an even higher impedance modulus of up to 8 GΩ cm^2, remaining stable for 21 days. This finding might be related to the higher overall connectivity of the BPO0.05 matrix, presenting highly polymerized organic moieties densely interconnected with reticulated silica nodes, supported by TG/DTG and mechanical testing.

Both hybrid matrices containing CNT and GO presented a higher level of corrosion resistance, and in the case of GO incorporation also a prolonged lifetime of up to 29 weeks. The excellent corrosion resistance of the BPO0.01_GO coating was confirmed by the time evolution of Nyquist and Bode plots, shown in Figure 9. Following the work of Kuhn at al. [12], who studied the role of CNTs in epoxy composite films, it can be suggested that the carbon nanostructures embedded in PSS matrix act as densifier of the nanocomposite structure, thus providing improved barrier properties against the penetration of electrolytes in the coating. Once again, the two-dimensionality of GO structure provides better barrier effect compared to CNTs, increasing the pathway of the electrolyte to reach the metal substrate. An additional protection mechanism

might be related to the increase of the ionic resistance of the coatings by the presence of carbon nanostructures [14,15]. In this case, the negatively charged GO and CNTs act as repulsive agents for the chloride anions, resulting in an improved barrier property of the coating.

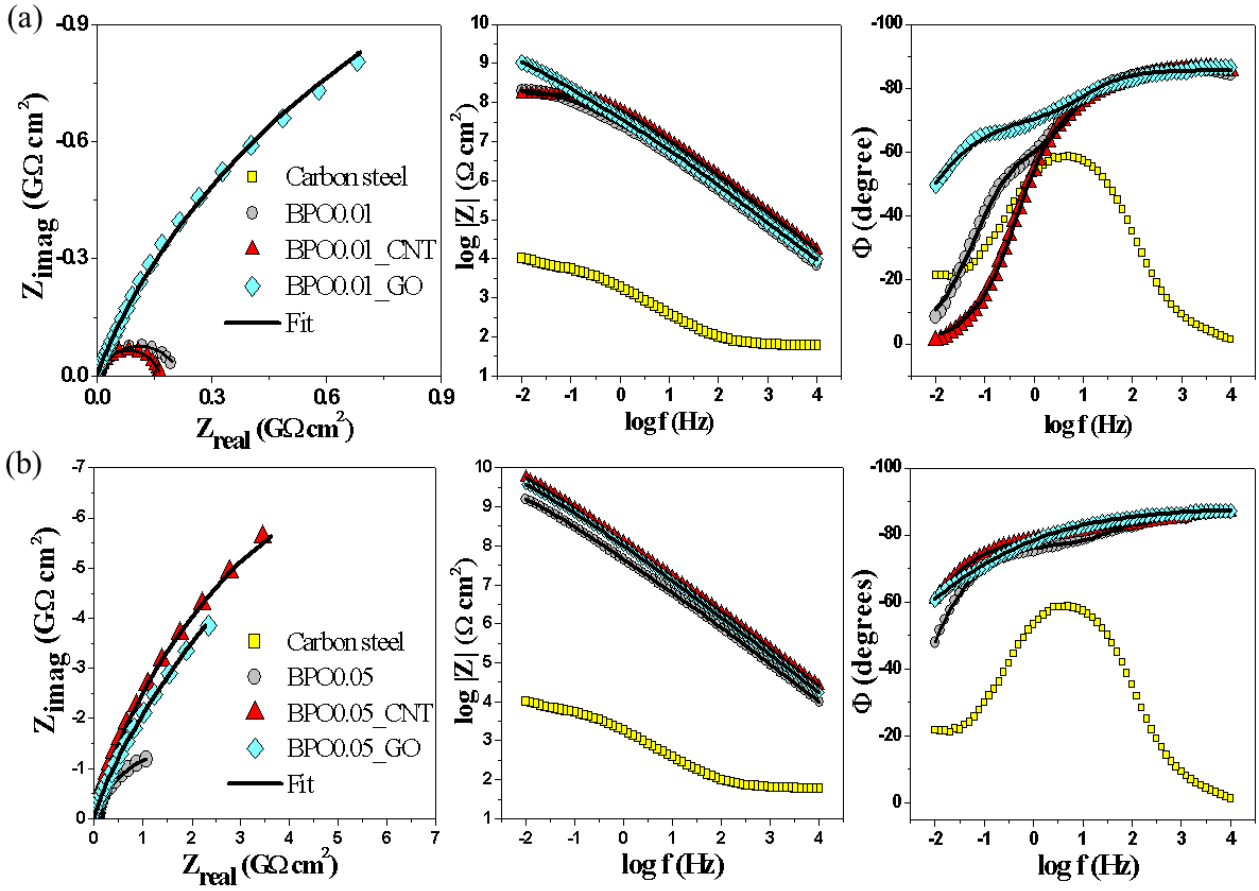

Figure 8. Nyquist and Bode plots of unloaded and CNT and GO loaded (a) BPO0.01 and (b) BPO0.05 matrix compared to bare carbon steel, after one day of immersion in 3.5 % NaCl solution.

The capacitance of the coating is indicative for the diffusion behavior of the electrolyte [15]. Low permeability towards corrosive electrolytes results in low capacitance values. To extract the capacitance values, the equivalent circuit, displayed in Figure 10, was used to fit the EIS data. It

contains a high frequency (~10^4 Hz) and low frequency (~0.1 Hz) time constants, with R_c and CPE_c being the resistance and capacitance of the coating, while R_{ct} and CPE_{dl} is the resistance to charge transfer and capacitance of the double layer at the coating/steel interface, respectively [36]. The parameters determined by fitting the EIS measurements are shown in Table 3.

The high value of the coating resistances (R_c) and the even higher charge transfer resistances (R_{ct}) are consequences of the densely packed hybrid network, which hinders the uptake of the electrolyte and its diffusion to the steel substrate. As only extremely small quantities of the electrolyte are able to reach the metal/coating interface, the formed double-layer has a very low capacitance and very high charge transfer resistance, in the range of several GΩ cm^2 for BPO0.05_GO samples (Table 3). The low values of the coating capacitance, C_c, calculated using Eq. 1, show that the dielectric hybrid layer acts as a capacitor, blocking the entrance of charged corrosive species into the coating. This behavior is also expressed by the n_c values, all close to unity, approaching the behavior of ideal capacitor (n ~ 1), and by the wide band in phase angle graph with values below -80° extending over a frequency range of 4 orders of magnitude.

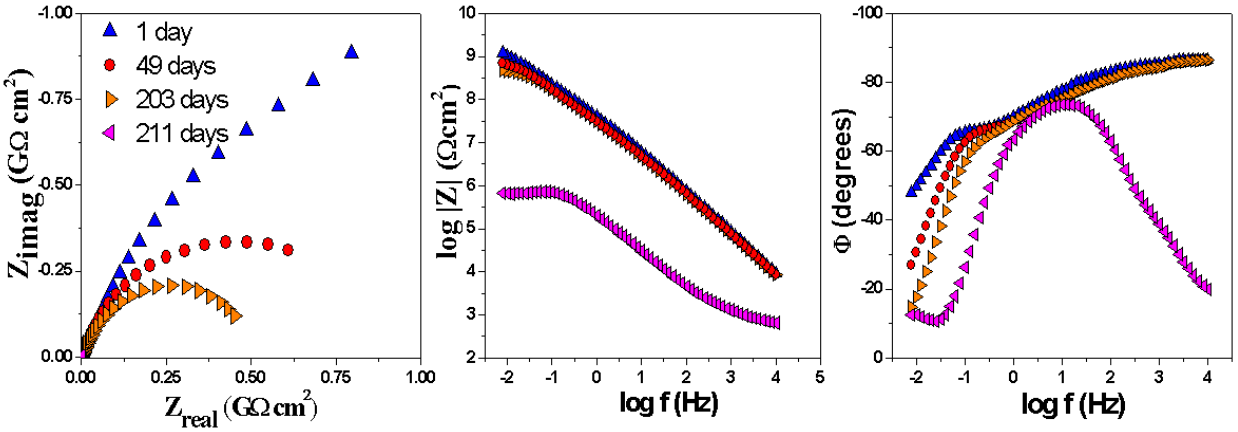

Figure 9. Nyquist and Bode plots for BPO0.01_GO sample deposited on carbon steel with immersion time dependence in 3.5 % NaCl standard saline solution.

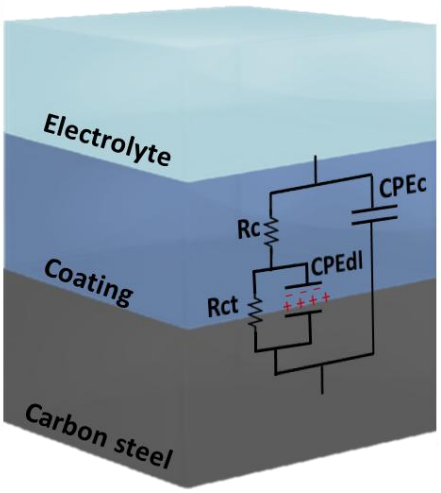

Figure 10. The electrical equivalent circuit used to fit all EIS experimental data.

Table 3. Electrochemical parameters derived by fitting of the EIS data, using the electrical circuit of Figure 10, for all hybrid coatings after one day immersion in saline NaCl 3.5% solution. The values in brackets correspond to the error (%) of each parameter.

Sample	BPO0.01	BPO0.01_ CNT	BPO00.1_ GO	BPO0.05	BPO0.05_ CNT	BPO00.5_ GO
χ^2	1.4×10^{-3}	3.0×10^{-4}	9.0×10^{-4}	3.0×10^{-4}	2.3×10^{-4}	1.4×10^{-4}
R_c ($M\Omega cm^2$)	28 (3.8)	13 (8.8)	29 (5.0)	15 (5.5)	10 (10)	4.6 (39)
Q_c ($n\Omega^{-1}cm^{-2}s^n$)	3.8 (1.0)	1.5 (1.0)	2.9 (0.9)	2.7 (0.8)	0.95 (1.2)	1.3 (1.4)
n_c	0.95 (0.1)	0.96 (0.1)	0.95 (0.2)	0.95 (0.1)	0.96 (0.1)	0.97 (0.1)
C_c ($nFcm^{-2}$)	3.4	1.3	2.5	2.3	0.78	1.1
R_{ct} ($G\Omega\ cm^2$)	0.19 (1.3)	0.16 (1.1)	0.22 (1.7)	3.8 (1.2)	26.2 (1.7)	46.8 (6.9)
Q_{dl}($n\Omega^{-1}cm^{-2}s^n$)	7.3 (1.5)	1.7 (1.3)	4.8 (1.5)	2.2 (0.9)	0.66 (1.8)	0.93 (1.7)
n_{dl}	0.74 (1.3)	0.65 (0.9)	0.68 (1.5)	0.70 (0.3)	0.70 (0.4)	0.60 (0.9)

The coating capacitances values as a function of immersion time in saline environment are presented in Figure 11. It is interesting to note that for both hybrid matrices the addition of GO

and in particular of CNTs decreases the coating capacitance as a result of the negatively charged carbon nanostructures, thus contributing to a improved barrier property of the coatings. Moreover, Figure 11a and 11b show that the coating capacitance quickly increases during initial period of immersion, which is attributed to the water uptake into the coatings. With prolonged immersion times a clear saturation behavior can be observed. The water uptake of the coatings, calculated from Eq. 2, is plotted as a function of immersion time in Figure 11c. Compared to the pure BPO0.01 matrix the incorporation of both GO and CNT reduced the water uptake of the coating. For BPO0.05_GO sample the uptake remains below 6 vol.% during the entire coating lifetime of 24 weeks. From these results it can be concluded that the addition of CNTs and GO in both matrices has a significant effect on the corrosion resistance of the coatings, expressed by the low values of coating capacitance and water uptake.

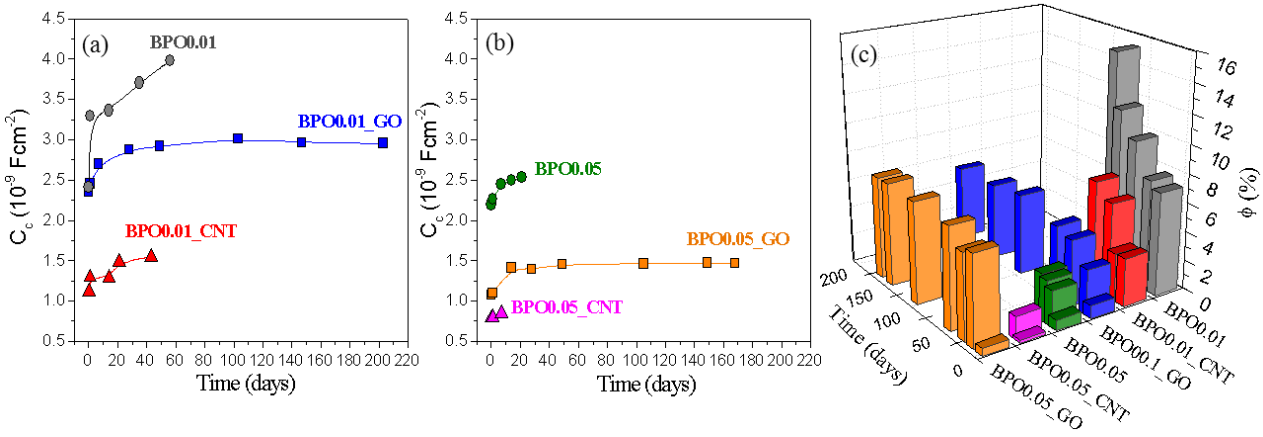

Figure 11. Immersion time dependence of the coating capacitances of the BPO0.01 matrix (a) and BPO0.05 matrix (b) containing CNTs and GO, extracted from fitting the EIS data. (c) Water uptake time dependence of all coatings.

Overall, all coatings showed a 4 - 6 orders of magnitude higher impedance modulus than uncoated carbon steel, highlighting the efficiency of the PMMA-siloxane-silica system as a protective coating. Compared to CNT or GO reinforced polymer coatings, reported so far, the PPS coatings studied in this work provide by far the most effective corrosion protection barrier of metallic alloys, with a significantly higher impedance modulus and lifetime in 3.5% NaCl medium. This extraordinary electrochemical performance, for films with only several micrometers in thickness, approaching the characteristics of thick paints, is related to their dense hybrid nanostructure, acting as efficient anticorrosive barrier [20].

Nevertheless, high performance protective coatings face the challenge of being able to resist simultaneously severe situations such as high temperatures, abrasive conditions and corrosive environments. Therefore the key result here is that the high corrosion resistance of the PMMA-siloxane-silica coatings can be combined with a significant improvement of the thermal and mechanical stability of the hybrid structure by the addition of carbon nanofillers, extending the applicability of these coatings to a wider range of environments. Comparing the effect of GO and CNTs is clear that due to its geometry GO contributes more for the improvement of thermal resistance, while CNTs account as rigid obstacles for a stronger mechanical reinforcement, both nanofillers contribute to an improvement of the corrosion resistance of the coatings.

CONCLUSIONS

Noticeable improvement of thermal and mechanical properties has been achieved by the uniform dispersion of carbon nanotubes and graphene oxide in PMMA-siloxane-silica nanocomposites. The hybrid sols containing CNTs and GO, deposited on A1020 carbon steel, yielded homogeneous and defect-free coatings, with very smooth surface (R_{RMS} < 0.5 nm) and

thicknesses in the range of 3 – 7 μm. Mechanical and thermal reinforcement of the coatings was achieved for both carbon nanofillers, producing significantly higher scratch resistant and adherent coating to the carbon steel substrate, particularly in the case of CNT addition, and a substantial increment of the thermal stability of 70 °C, found for GO coatings. Electrochemical impedance spectroscopy results showed that CNT and GO reinforced coatings act also as very efficient corrosion barrier, showing impedance modulus up to 8 GΩ cm^2. Here, GO containing coatings proved to be very effective in improving the impedance modulus and the long-term stability, up to 203 days in saline solution. From a technological point of view, the possibility of achieving a significant mechanical and thermal reinforcement effect of the PMMA-siloxane-silica matrix by incorporation of CNT and GO, is particularly promising for extending the applicability of these thin, environmentally compliant, high efficiency anticorrosive coatings to abrasive environments.

AUTHOR INFORMATION

Corresponding Author

*E-mail: peter@iq.unesp.br

Instituto de Química, Departamento de Físico-Química

Rua Prof. Francisco Degni, 55

CEP 14800-060, Araraquara/SP, Brazil

+55 16 33019887

Author Contributions

S.V.H. is the main author contributing in all steps. S.H.P. and C.V.S. worked on results discussion. K.M.K. planned and discussed the mechanical experiments in this work. P.H. (supervisor of S.V.H.) suggested the experiments, discussed the results and wrote together with S.V.H. the manuscript. All the authors read and commented on the manuscript.

ACKNOWLEDGMENT

We would like to thank John Nunn from the National Physical Laboratory, England, for access to the microscratch equipment. This work was supported by CNPq, CAPES and FAPESP. The FAPESP scholarships processes were 2014/12182-9 and 2013/04314-0.

ABBREVIATIONS

MMA, methyl methacrylate; PMMA, poly(methyl methacrylate); TEOS, tetraethoxysilane; MPTS, 3-(trimethoxysilyl)propyl methacrylate; OCP, open circuit potential; CNT, carbon nanotube; GO, graphene oxide; PSS, PMMA-Siloxane-Silica; EIS, electrochemical impedance spectroscopy; FEG-SEM, field emission scanning electron microscope; AFM, atomic force microscopy; XPS, X-ray photoelectron spectroscopy.

REFERENCES

1 Iijima, S. Helical Microtubules of Graphitic Carbon. *Nature* **1991**, *354*, 56-58.

2 Novoselov, K. S.; Geim, A. K.; Morozov, S. V.; Jiang, D.; Zhang, Y.; Dubonos, S. V.; Grigorieva, I. V.; Firsov, A. A. Electric Field Effect in Atomically Thin Carbon Films. *Science* **2004**, *306*, 666-669.

3 Voiry, D.; Vallés, C.; Roubeau, O.; Pénicaud, A. Dissolution and Alkylation of Industrially Produced Multi-Walled Carbon Nanotubes. *Carbon* **2011**, *49*, 170-175.

4 Alves da Cunha, J. R.; Fantini, C.; Andrade, N. F.; Alcantara, P.; Saraiva, G. D.; Filho, A. G. S.; Terrones, M.; Santos, M. C. Dos. Enhanced Solubilization of Carbon Nanotubes in Aqueous Suspensions of Anionic−Nonionic Surfactant Mixtures. *J. Phys. Chem. C* **2013**, *117*, 25138–25145.

5 Chen, L.; Chai, S.; Liu, K.; Ning, N.; Gao, J.; Liu, Q.; Chen, F.; Fu, Q. Enhanced Epoxy/Silica Composites Mechanical Properties by Introducing Grapheme Oxide to the Interface. *ACS Appl. Mater. Interfaces* **2012**, *4*, 4398-4404.

6 Xiong, J.; Zheng, Z.; Qin, X.; Li, M.; Li, H.; Wang, X. The Thermal and Mechanical Properties of a Polyurethane/Multi-Walled Carbon Nanotube Composite. *Carbon* **2006**, *44*, 2701-2707.

7 Mallakpour, S.; Zadehnazari. A. Preparation of Dopamine-Functionalized Multi-Wall Carbon Nanotube/Poly(Amide-Imide) Composites and their Thermal and Mechanical Properties. *New Carbon Mater.* **2016**, *31*, 18–30.

8 Wang, J.; Shi, Z.; Ge, Y.; Wang, Y.; Fan, J.; Yin, J. Solvent Exfoliated Graphene for Reinforcement of PMMA Composites Prepared by In Situ Polymerization. *Mater. Chem. Phys.* **2012**, *136*, 43–50.

9 Mohamadi, S.; Sharifi-Sanjani, N.; Mahdavi, H. Functionalization of Graphene Sheets via Chemically Grafting of PMMA Chains Through In-Situ Polymerization. *J. Macromol. Sci., Part A: Pure Appl.Chem.* **2011**, *48*, 577-582.

10 Gojny, F. H.; Wichmann, M. H. G.; Köpke, U.; Fiedler, B.; Schulte, K. Carbon Nanotube-Reinforced Epoxy-Composites: Enhanced Stiffness and Fracture Toughness at Low Nanotube Content. *Compos. Sci. Technol.* **2004**, *64*, 2363–2371.

11 Jeon, H.; Park, J.; Shon, M. Corrosion Protection by Epoxy Coating Containing Multi-Walled Carbon Nanotubes. *J. Ind. Eng. Chem.* **2013**, *19*, 849-853.

12 Khun, N. W.; Troconis, B. C. R.; Frankel, G. S. Effects of Carbon Nanotube Content on Adhesion Strength and Wear and Corrosion Resistance of Epoxy Composite Coatings on AA2024-T3. *Prog. Org. Coat.* **2014**, *77*, 72–80.

13 Chang, K-C; Hsu, M-H; Lu, H-I; Lai, M-C; Liu, P-J; Hsu, C-H; Ji, W-F; Chuang, T-L; Wei, Y.; Yeh, J-M; Liu, W-R; Room-Temperature Cured Hydrophobic Epoxy/Graphene Composites as Corrosion Inhibitor for Cold-Rolled Steel. *Carbon* **2014** *6*, 144–53.

14 Ramezanzadeh, B.; Niroumandrad, S.; Ahmadi, A.; Mahdavian, M.; Moghadam, M. H. M. Enhancement of Barrier and Corrosion Protection Performance of an Epoxy Coating through Wet Transfer of Amino Functionalized Graphene Oxide. *Corros. Sci.* **2016**, *103*, 283–304.

15 Ramezanzadeh, B.; Ghasemi, E.; Mahdavian, M.; Changizi, E.; Mohamadzadeh Moghadam, M. H. Covalently-Grafted Graphene Oxide Nanosheets to Improve Barrier and Corrosion Protection Properties of Polyurethane Coatings. *Carbon* **2015** *93,* 555 – 573.

16 Case Study, Forth Rail Bridge United Kingdom, *The Sherwin-Williams Company* **2013**.

17 Clarke, D. R.; Phillpot, S. R. Thermal Barrier Coating Materials. *Mater. Today* **2005**, 22-29.

18 Hammer, P.; Santos, F. C. Dos; Cerrutti, B. M.; Pulcinelli, S. H.; Santilli, C. V. Highly Corrosion Resistant Siloxane-Polymethyl Methacrylate Hybrid Coatings. *J. Sol-Gel Sci. Technol.* **2012***,* 63, 266-274.

19 Sanchez, C.; Belleville, P. ; Popall, M.; Nicole, L. Applications of Advanced Hybrid Organic-Inorganic Nanomaterials: from Laboratory to Market. *Chem. Soc. Rev.* **2011**, *40*, 696-753.

20 Santos, F. C. Dos; Harb, S. V.; Menu, M.; Turq, V.; Pulcinelli, S. H.; Santilli, C. V.; Hammer, P. On the Structure of High Performance Anticorrosive PMMA-siloxane-silica Hybrid Coatings. *RSC Adv.* **2015**, *5*, 106754-106763.

21 Hammer, P.; Santos, F. C. Dos; Cerrutti, B. M.; Pulcinelli, S. H.; Santilli, C. V. Carbon Nanotube-Reinforced Siloxane-PMMA Hybrid Coatings with High Corrosion Resistance. *Prog. Org. Coat.* **2013**, *76*, 601–608.

22 Hirschorn, B.; Orazem, M. E.; Tribollet, B.; Vivier, V.; Frateur, I.; Musiani, M. Determination of Effective Capacitance and Film Thickness from Constant-Phase-Element Parameters. *Electrochim. Acta* **2010**, *55* 6218–6227.

23 Córdoba, L. C.; Montemor, M. F.; Coradin, T. Silane/TiO2 Coating to Control the Corrosion Rate of Magnesium Alloys in Simulated Body Fluid. *Corros. Sci.* **2016**, *104*, 152–161.

24 Brasher, D. M.; Kingsbury, A. H. Electrical Measurements in the Study of Immersed Paint Coatings on Metal. I. Comparison Between Capacitance and Gravimetric Methods of Estimating Water-Uptake. *J. Appl. Chem. Biotechnol*. **1954**, *4,*, 62-72.

25 Malmberg, C. G.; Maryott, A. A.; Dielectric Constant of Water from 0° to 100° C. *J. of Res. of the Nat. Stand.* **1956**, *56*, 1-8.

26 Briggs D., Seah M.P., editors. Practical Surface Analysis: Auger and X-Ray Photoelectron Spectroscopy. 2nd ed. Chichester: Wiley; 1990. 674 p.

27 Wang, Y. T.; Chang, T. C.; Hong, Y. S.; Chen, H. B. Effect of the Interfacial Structure on the Thermal Stability of Poly(Methyl Methacrylate)-Silica Hybrids. *Thermochim. Acta* **2003**, *397*, 219-226.

28 Kashiwagi, T.; Inaba, A.; Brown, J. E.; Hatada, K.; Kitayama, T.; Masuda, E. Effects of Weak Linkages on the Thermal and Oxidative Degradation of Poly(Methyl Methacrylates). *Macromol* **1986**, *19*, 2160-2168.

29 Jin, Z.; Pramoda, K. P.; Xu, G.; Goh, S. H. Dynamic Mechanical Behavior of Melt-Processed Multi-Walled Carbon Nanotube/Poly(Methyl Methacrylate) Composites. *Chem. Phys. Lett.* **2001**, *337*, 43–47.

30 Potts, J. R.; Dreyer, D. R.; Bielawski, C. W.; Ruoff, R. S. Graphene-Based Polymer Nanocomposites. *Polym*. **2011**, *52*, 5-25.

31 Pham, V. H.; Dang, T. T.; Hur, S. H.; Kim, E. J.; Chung, J. S. Highly Conductive Poly(Methyl Methacrylate) (PMMA)-Reduced Graphene Oxide Composite Prepared by Self-Assembly of PMMA Latex and Graphene Oxide through Electrostatic Interaction. *ACS Appl. Mater. Interfaces* **2012**, *4*, 2630-2636.

32 Paul, D. R.; Robeson, L. M. Polymer Nanotechnology: Nanocomposites. *Polym*. **2008**, *49*, 3187-3204.

33 Zhang, T.; Du, Z.; Zou, W.; Li, H.; Zhang, C. The Flame Retardancy of Blob-Like Multi-Walled Carbon Nanotubes/Silica Nanospheres Hybrids in Poly (Methyl Methacrylate). *Polym. Degrad. Stabil.* **2012**, *97*, 1716-1723.

34 Bao, C.; Guo, Y.; Yuan, B.; Hu, Y.; Song, L. Functionalized Graphene Oxide for Fire Safety Applications of Polymers: a Combination of Condensed Phase Flame Retardant Strategies. *J. Mater. Chem*. **2012**, *22*, 23057-23063.

35 Carvalho, H. W. P.; Suzana, A. F.; Santilli, C. V.; Pulcinelli, S. H. Synthesis, Structure, and Thermal Stability of Poly(methyl methacrylate)-co-Poly(3-tri(methoxysilyil)propyl methacrylate)/ Montmorillonite Nanocomposites. *Polymer Energneering and Science – 2013*, **2013**, 1253-1261.

36 Mansfel, F. Electrochemical Impedance Spectroscopy (EIS) as a New Tool for Investigating Methods of Corrosion Protection. *Electrochim. Acta* **1990**, *35*, 1533-1544.

Table of Contents Graphic